minerals

Article

Chronological and Mineralogical Records of the Langqi Pluton, Fuzhou: Constraints on the Magma Mixing Process

Zhouxin Chen, Liyuan Wang * and Xue Yan

Zijin School of Geology and Mining, Fuzhou University, Fuzhou 350108, China; chenzhouxin0718@163.com (Z.C.); 15880445655@163.com (X.Y.)
* Correspondence: wangliyuan030101@163.com

Abstract: The mafic microgranular enclaves (MMEs) from Mesozoic intermediate-acid magmatic rocks, widely developed along the Fujian coast, are considered to be the results of large-scale crust–mantle interaction by magma mixing. This paper is based on zircon U-Pb chronology, along with zircon Hf isotope and mineral analyses for the host granite and MMEs from Langqi Island, in order to investigate the magma mixing mechanism of the Langqi pluton in Fuzhou, Southeast China. The results indicate that the MMEs were emplaced during the late Early Cretaceous (98.9 ± 2.2 Ma), identical to the age of the granite (100.1 ± 1.1 Ma) within the error range. The zircon εHf(t) values for the granite and MMEs are in the ranges of −2.1~0.0 and −1.7~+1.1. The zircon Hf isotope data indicate that both the granite and MMEs were predominantly derived from the ancient crustal basement of Cathaysia, with a partial mantle-derived contribution. The An values of plagioclase phenocrysts with oscillatory zoning patterns in the MMEs show oscillatory changes from the core to the rim, indicating multiple mixing events between the two magmas with different compositions. Amphiboles in the MMEs show characteristics of crust–mantle contamination, and the Ti migrated from the mafic magma with high concentration to the felsic magma with low concentration during the magma mixing process. Biotites in the host rock and MMEs belong to primary biotite, and they have relatively high MgO contents (ave. 12.78 wt.%) and relatively low $FeO^T/(MgO + FeO^T)$ ratios (ave. 0.56), showing characteristics of crust–mantle contamination. The crust–mantle magma interaction in a crystal, mushy state played a significant role in controlling the formation and evolution of the Langqi pluton. The magmatism was predominantly sourced from mixing between the mantle-derived mafic magma and the crust-derived felsic magma during the subduction of the Paleo-Pacific Plate, resulting in the formation of the Langqi doleritic veins, granites, and MMEs.

Keywords: mafic microgranular enclaves; chronology; mineralogy; magma mixing; Langqi Island

check for updates

Citation: Chen, Z.; Wang, L.; Yan, X. Chronological and Mineralogical Records of the Langqi Pluton, Fuzhou: Constraints on the Magma Mixing Process. *Minerals* **2023**, *13*, 1538. https://doi.org/10.3390/min13121538

Received: 22 September 2023
Revised: 7 December 2023
Accepted: 8 December 2023
Published: 11 December 2023

1. Introduction

Significant tectonic events have occurred in South China since the Jurassic period, resulting in multiple phases of magmatic activity that exhibit episodic characteristics [1–3]. Based on the chronological data of more than 780 Jurassic–Cretaceous igneous rocks in South China [4], the magmatism can be classified into four main phases: 190~175 Ma, 165~155 Ma, 145~125 Ma, and 105~95 Ma, with corresponding peak times of magmatism at 160, 130, and 100 Ma, of which the first two phases are mainly Jurassic intrusive magmatism in inner South China, while the last two phases are mainly Cretaceous volcanic magmatism in the southeast coastal region of China. Understanding the origin of the extensively exposed igneous rocks in this region holds immense importance in interpreting the crust–mantle interaction, formation and evolution of the crust, and geodynamic processes. During the subduction of the Paleo-Pacific Plate, the subduction angle became larger due to slab rollback, which enhanced the thermal flux cycle in the subcontinental lithosphere. The induced mantle-derived magma underplating may be the formation mechanism of intermediate-acid intrusive rocks in the region [3–5]. Hence, both mantle-derived magma underplating and crust–mantle magma mixing played a pivotal role in the genesis of Late Mesozoic igneous rocks in South China. The Cretaceous crust–mantle interaction was intense in the Fujian coastal region, and the intermediate-acid volcanic–intrusive rocks were formed through varying degrees of mixing of the mantle-derived magma and subsequently induced crustal felsic magma by underplating.

Mafic microgranular enclaves (MMEs) developed in intermediate-acid granitic rocks are regarded as an indicator of magma mixing [6–8]. Magma mixing, a significant process in magma's evolution, operates widely in tectonic settings such as active continental margins, collisional orogenic belts, and continental rifts. It is one of the main reasons for the diversity of igneous rocks and is of great importance in understanding the genesis of granites and geodynamic processes [9].

The MMEs are very common in the granite of Langqi Island, Fuzhou. According to Huang et al. (2020) [10], the Langqi granite and its MMEs exhibit characteristics of magma mixing as determined by whole-rock geochemical analysis. However, a comprehensive understanding of the origin of these rocks is impeded by the lack of research on the formation age of the MMEs and the mineral chemistry of the Langqi pluton. The study of magma interaction in the Langqi granite and MMEs is of great significance for understanding the Late Mesozoic tectonic evolution process in the coastal areas of Fujian. The minerals in the granitic rocks (such as plagioclase, amphibole, biotite, etc.) undergo the entire process of magma evolution, and their chemical compositional characteristics can effectively trace the mixing process of the magma, recording the physical and chemical conditions of the magma formation process and magma evolution information [11–13]. In this study, we present geochronological, Hf isotopic, and mineral chemistry (plagioclase, amphibole, and biotite) for the host granite and MMEs from Langqi Island, in order to determine the physical and chemical conditions of mineral formation and, thus, explore the mechanism and process of magma mixing in the Langqi pluton.

2. Geological Setting

The coastal area of Fujian in the eastern Cathaysia Block is characterized by large-scale Late Mesozoic tectonic–magmatic activities, such as the intrusion of A-type granites [5], mafic dykes [14], and I-A-type composite granites, which are closely related to the subduction of the Paleo-Pacific Plate [15]. The prevalence of I-A-type composite granites in the region indicates a shift from compressional to extensional environments [5,16,17]. Furthermore, the ages of igneous rocks in the southeast coastal region show a trend of becoming younger from the inland to the ocean, while the zircon Hf isotope composition gradually shifts from enrichment to depletion from the early to late periods [18]. This suggests that the involvement of mantle material in the formation of Late Mesozoic rocks in the southeastern coastal region increased progressively.

The study area is located on Langqi Island in Fuzhou, which is in the eastern part of the Cathaysia Block. Tectonically, it is located in the eastern part of the Changle-Nan'ao Fault Zone (Figure 1a), which is a large-scale northeast–southwest-trending sinistral strike-slip fault zone that has developed in the region. Granites and mafic dyke swarms are common on Langqi Island. The exposed stratigraphy on the island includes the Upper Jurassic Nanyuan Formation, the Lower Cretaceous Xiaoxi Formation, and Quaternary strata (Figure 1b). The lithology of the Langqi pluton mainly consists of granite with MMEs (Figure 2a–f) and doleritic veins (Figure 2g–i). The samples for this study were collected from the southeastern region of Langqi Island (Figure 1b), including the host granite and MMEs. The host granites were formed in the late Early Cretaceous, and they exhibit mineralogical and chemical characteristics of I-type granite. The host granites and MMEs are significantly enriched in light rare-earth and large-ion lithophile elements, while they are depleted in heavy rare-earth and high-field-strength elements [10], indicating a signature of arc magma and suggesting the formation of the Langqi pluton in a subduction environment. This is consistent with the continuous subduction of the Paleo-Pacific Plate during the Middle Jurassic to Early Cretaceous.

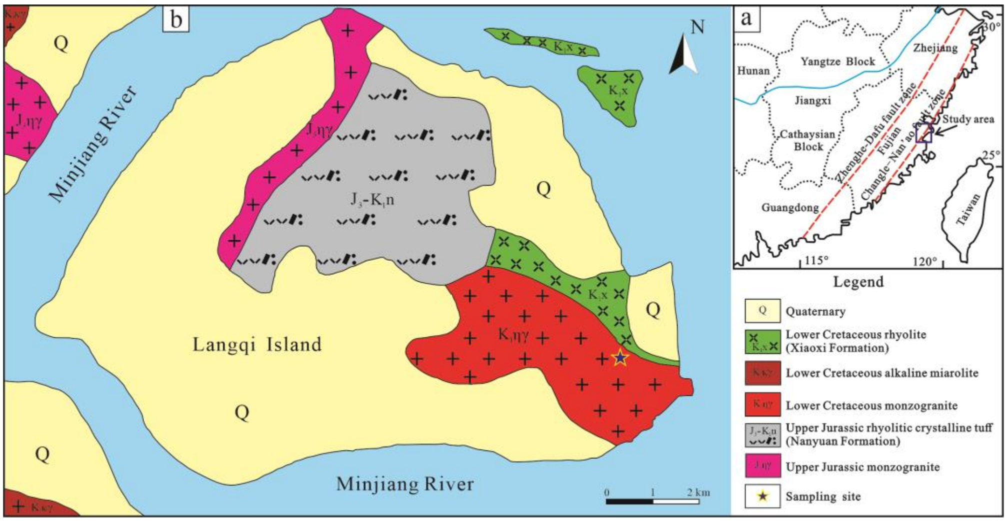

Figure 1. Sketch map of Fujian Province ((**a**), after Wang et al., 2020) [18] and geological map of the Langqi region ((**b**), after Huang et al., 2020) [10].

Figure 2. Field characteristics of Langqi pluton: (**a**,**c**) Plagioclase phenocrysts in the MMEs exhibit shapes and sizes comparable to those present in the host rock. (**b**,**d**) Smaller MMEs are enveloped by larger MMEs. (**e**) The MMEs are widely developed in granite, mainly lenticular and ellipsoidal. (**f**) The contact between the MMEs and the host granite is sharp. (**g**–**i**) The doleritic veins developed in the granite on both sides are greyish-green in color.

3. Field Relations and Petrography

The MMEs widely developed in the granite are mainly lenticular and ellipsoidal, with diameters ranging from 3 to 20 cm (Figure 2a–f). The contact between the MMEs and the host granite varies from gradual to sharp. Plagioclase phenocrysts in the MMEs are similar in size and shape to the plagioclases in the host granite (Figure 2a,c). The phenomenon of larger MMEs enveloping smaller MMEs can occasionally be seen (Figure 2b,d). The doleritic veins developed in the granite on both sides are greyish-green in color and approximately 3–10 m in length (Figure 2g–i).

The host granites are mainly gray, with medium-coarse grains, which have a massive structure and a porphyritic texture. The rocks mainly consist of K-feldspar (ca. 40%), quartz (ca. 30%), plagioclase (ca. 25%), and biotite (ca. 4%), with accessory minerals such as zircon and titanite. The K-feldspar is anhedral and tabular, with intense kaolinization alterations (Figure 3a,b). Plagioclase exhibits a euhedral or subhedral and tabular texture, generally develops polysynthetic twins (Figure 3c), and often develops sericitization in the interior of the plagioclase. Biotites are widely distributed in other minerals in the form of euhedral and subhedral crystals (Figure 3a–c), and they are occasionally altered into epidote. The host granite shows no visible amphiboles.

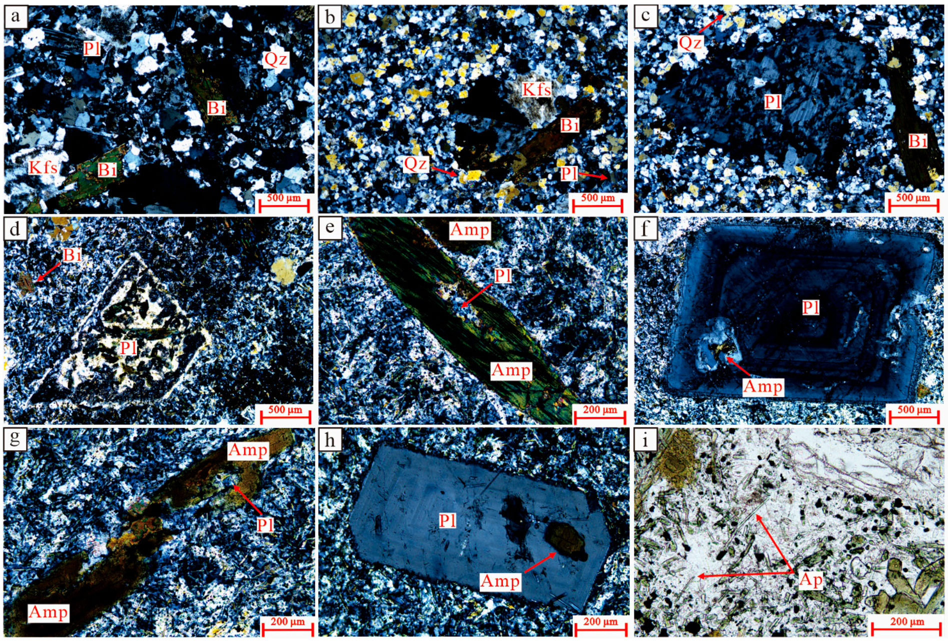

Figure 3. Microscopic photos of the Langqi pluton: (**a**–**c**) Granite has a porphyritic texture. (**d**) Microstructures of the MMEs, the poikilitic inclusions of amphibole within the plagioclase with a chaotic texture. (**e**,**g**) Microstructures of the MMEs, the poikilitic inclusions of plagioclase within the amphibole with a long column shape. (**f**,**h**) Microstructures of the MMEs, the poikilitic inclusions of amphibole within the plagioclase with an oscillatory zoning pattern. (**i**) The needle-shaped apatite in the MMEs (Pl—plagioclase; Qz—quartz; Kfs—K-feldspar; Amp—amphibole; Bi—biotite; Ap—apatite).

The mineral grain sizes within the MMEs are generally smaller than those of the host granites. The MMEs are mainly dioritic in composition and have a massive structure and a porphyritic index of ca. 10%. The phenocrysts are mainly plagioclase (ca. 50%), amphibole (ca. 25%), biotite (ca. 15%), and quartz (ca. 5%). The plagioclase phenocrysts can be divided into two types: the first type is euhedral, subhedral, and chaotic in texture, filled with poikilitic inclusions of amphibole in melting embayments and holes (Figure 3d), while the second type is euhedral plagioclase with an oscillatory zoning pattern, also filled with the poikilitic inclusions of amphibole (Figure 3f,h), indicating a multistage growth of plagioclase phenocrysts. The amphiboles are often euhedral and mostly brown in color, displaying pleochroism. A portion of the amphiboles show long prismatic crystals and are characterized by a diagnostic brownish-green color and the poikilitic inclusions of plagioclase within their cores (Figure 3e,g). The biotites are dark brown in color and show euhedral morphologies, with distinct pleochroism. Needle-shaped apatite with an aspect ratio greater than 10:1 can also be observed distributed in the matrix (Figure 3i).

4. Analytical Methods and Results

4.1. Zircon U-Pb Dating

The zircon U-Pb dating of the MMEs (BT-1) was performed at the Wuhan Sample Solution Analytical Technology Co., Ltd., Wuhan, China. The U-Pb dating of zircon was performed using Agilent 7900 ICP-MS (Stevens Creek Blvd Santa Clara, CA, USA) and the laser ablation system Geolas Pro (Stevens Creek Blvd Santa Clara, CA, USA). The laser energy was 80 mJ/cm^2, with a frequency of 5 Hz and a laser spot diameter of 32 µm. Zircon 91500 and NIST610 glass were used as external standards for U-Pb dating. The detailed operating process and data reduction were the same as described by Liu et al. (2008) [19].

The zircons from MMEs are mainly colorless, transparent to translucent, and subhedral to euhedral columnar. They are 50–150 µm in length and 50–100 µm in width, and the ratios of length to width are between 1:1 and 3:1. The cathodoluminescence images reveal that almost all of the crystals have a clear oscillatory zoning (Figure 4a). Analytical results are provided in Supplementary Table S1. These zircons have U contents of 18–127 ppm, Th concentrations of 21–409 ppm, and Th/U ratios of 1.02–3.23, indicating that they are magmatic zircons. The $^{206}Pb/^{238}U$ ages obtained for the eighteen zircon grains from the MMEs (BT-1) are 97–103 Ma, with a weighted mean age of 98.9 ± 2.2 Ma (MSWD = 0.15, confidence = 0.95; Figure 4c), representing the crystallization age of the MMEs, which is consistent with the crystallization age of the host granite within the error range (100.1 ± 1.1 Ma, MSWD = 0.93; Figure 4d) [10].

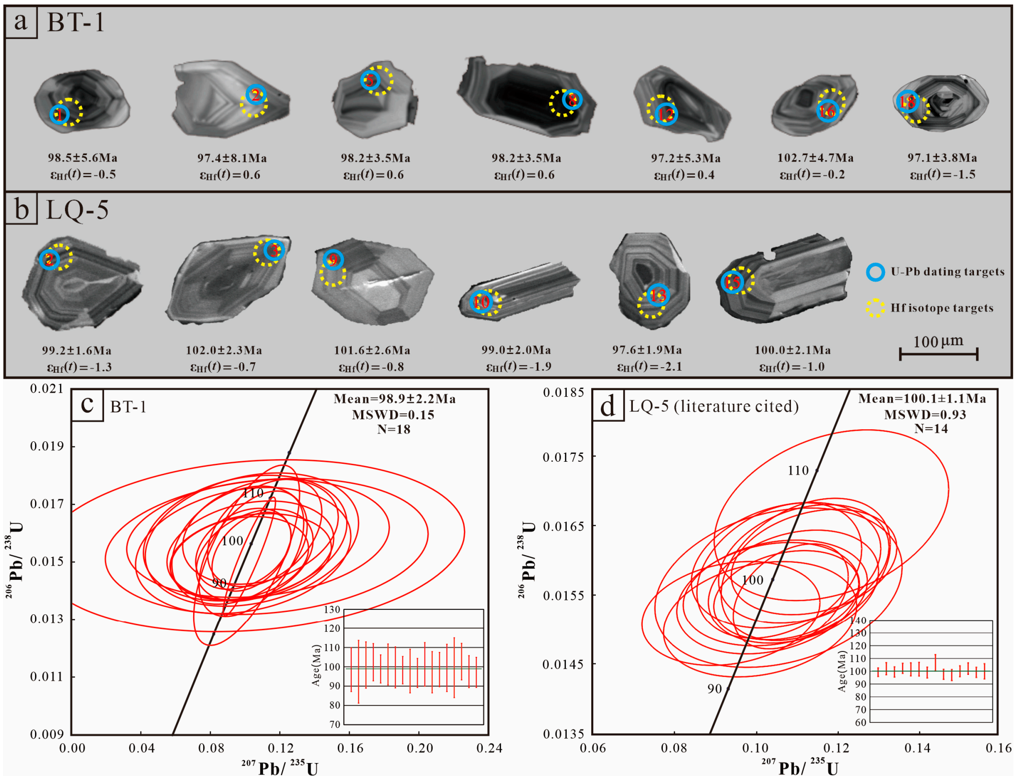

Figure 4. Cathodoluminescence (CL) images of representative zircon grains from (**a**) MME (BT-1) and (**b**) host granite (LQ-5) analyzed for U-Pb and Hf isotope ratios. Circles represent the U-Pb and Hf isotope analyses. (**c**) U-Pb concordia diagram of the MMEs; the inset in the figure shows the average mean age. (**d**) U-Pb concordia diagram of the host granite; the inset in the figure shows the average mean age (after Huang et al., 2020) [10].

4.2. Zircon Hf Isotope

The zircon Hf isotope analysis was performed at Wuhan Sample Solution Analytical Technology Co., Ltd., Wuhan, China, using a Neptune Plus MC-ICP-MS (Thermo Fisher

Scientific, Dreieich, Germany) equipped with a GeoLas HD laser ablation system (Coherent, Göttingen, Germany). Helium was used as the ablation carrier gas, with a laser beam diameter of 44 μm, energy of 8 mJ/cm^2, and frequency of 8 Hz. The Zircon 91500 and GJ-1 were used for monitoring the Hf isotope interference correction during the analysis process. The detailed operating process and data reduction were the same as described by Wu et al. (2006) [20].

Fourteen Lu-Hf analyses were performed for sample LQ-5 and eighteen analyses were performed for sample BT-1, located near the zircon U-Pb dating spots (Figure 4a,b). Analytical results are provided in Supplementary Table S2. The initial ^{176}Hf/^{177}Hf ratios of zircon grains from the host rock (LQ-5) varied from 0.282658 to 0.282712, while the εHf(t) values ranged between −2.1 and 0.0. The single-stage model ages (T_{DM1}) ranged from 775 to 884 Ma, and the two-stage model ages (T_{DM2}) ranged from 1162 to 1289 Ma. The MMEs (BT-1) had Hf isotope compositions similar to those of the host rock, with initial ^{176}Hf/^{177}Hf ratios of 0.282667~0.282745. The εHf(t) values of the MMEs ranged from −1.7 to +1.1, and the corresponding T_{DM1} and T_{DM2} values ranged from 732 to 863 Ma and 1089 to 1269 Ma, respectively. Although both samples had similar εHf(t) values, overall the host rock had a more enriched Lu–Hf isotope ratio than the MMEs.

4.3. Mineral Chemical Characteristics

The major element compositions of the minerals were determined using a JEOL JXA-8230 electron probe microanalyzer (EPMA) (Shimadzu, Tokyo, Japan) with ZAF matrix correction at Fuzhou University in Fujian. The operating conditions were 15 kV accelerating voltage, 20 nA beam current, 1–5 μm beam diameter, and a count time of 10 s. We used natural mineral standards for the Si, Al, Ca, Mg, Fe, Ti, K, Na, Mn, and P analyses. The probe data analysis and calculation were completed using GeokitPro (Build20220602) software.

4.3.1. Plagioclase

EMPA core–rim transect analysis was performed in representative plagioclases (mostly zoned phenocrysts and matrix crystals) of both MMEs and the host granite. The representative compositions and plagioclase formulae are provided in Supplementary Table S3. The An contents of plagioclase in the granite ranged from 6.7% to 27.8%, while those in the MMEs ranged from 10.8% to 57.2%. Compared with the host rock, the An content ranges of plagioclase in the MMEs were more variable. In the feldspar ternary diagram, the plagioclases in the host rock fall in the albite and oligoclase area, while the plagioclases in the MMEs fall in the albite–labradorite area (Figure 5a).

Plagioclase phenocrysts in the MMEs show an oscillatory zoning pattern, with a prominent calcic core. Along the boundary between the interior and the rim, dusty zones containing numerous minute tubular glass inclusions are common, and the zones truncate inner growth zoning. The variation trend of An contents from the core to the rim shows slight oscillatory zonings characterized by alternating decreases and increases (An = 28.0%→24.4%→25.4%→23.8%→26.3%→19.4%). The An contents of the plagioclase in the matrix (An = 10.8%–16.1%) are lower than those at the rim of the phenocryst (Figure 6).

4.3.2. Amphibole

Profile EMPA analysis was performed in representative amphibole phenocrysts from the MMEs. The representative compositions and plagioclase formulae are provided in Supplementary Table S4. The amphiboles in the MMEs are silica-poor, with relatively low SiO_2 contents (41.78–46.10 wt.%) and relatively high Al_2O_3 contents (8.48–11.17 wt.%), FeO contents (10.66–12.58 wt.%), MgO contents (12.31–14.92 wt.%), and CaO contents (9.96–11.10 wt.%). The Ca_B of all amphiboles in the MMEs is greater than 1.5, (Na_A + K_A) is greater than 0.5, and based on the nomenclature [21], most amphiboles in the MMEs plot at the boundary of edenite and pargasite, with a small amount of magnesiohastingsite (Figure 5b). The profiles across amphibole phenocryst show that the contents of Na_2O, MgO, and Al_2O_3 change slightly from the core to the rim of the phenocryst, while the content of TiO_2 exhibits a distinct uneven pattern of "high content at the core and low content at the rim" (Figure 7).

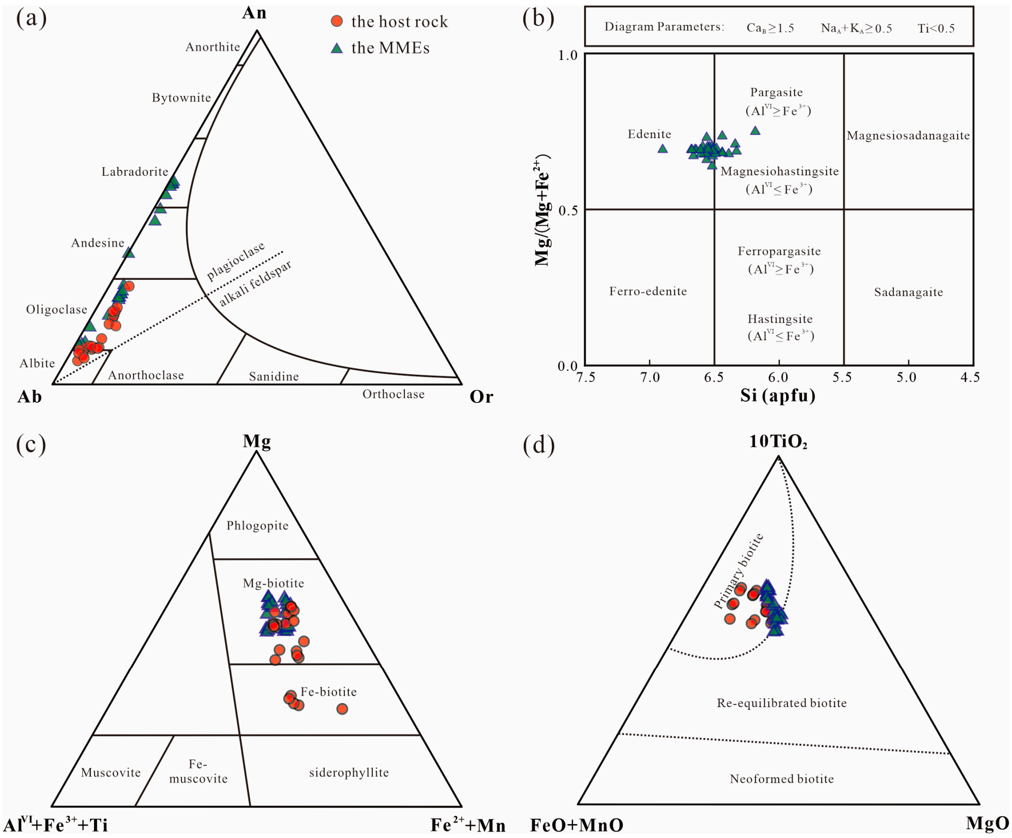

Figure 5. Compositions of minerals of the host rock and MMEs from Langqi pluton: (**a**) Feldspar ternary diagram showing the chemical composition of the studied plagioclase from the host rock and MMEs. (**b**) Mg/(Mg + Fe^{2+}) versus Si diagram of the studied amphibole from the MMEs (after Leake et al., 1997) [21]. (**c**) Classification diagram of biotites from the host rock and MMEs (after Forster, 1960) [22]. (**d**) Genetic diagram of biotites from the host rock and MMEs (after Nachit et al., 2005) [23].

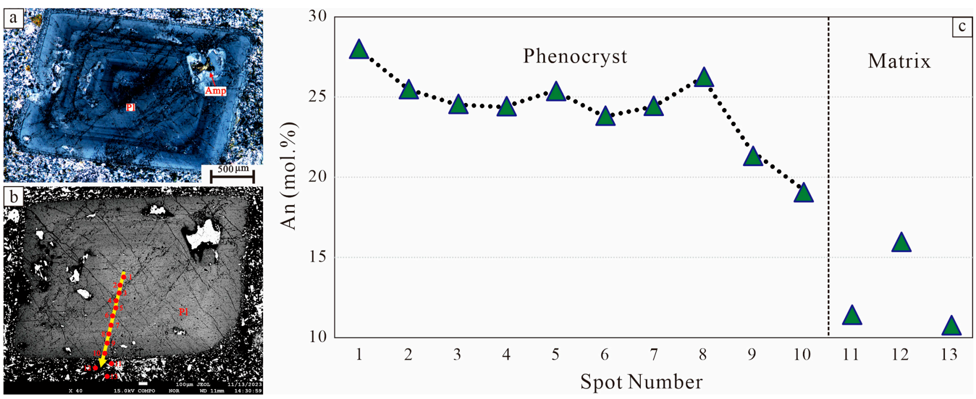

Figure 6. (**a**) Representative transmitted light microphotographs, (**b**) BSE images and (**c**) profile An (mol%) variations along traverses of the plagioclase from the MMEs. The red dots are the spots of the electron microprobe analyses.

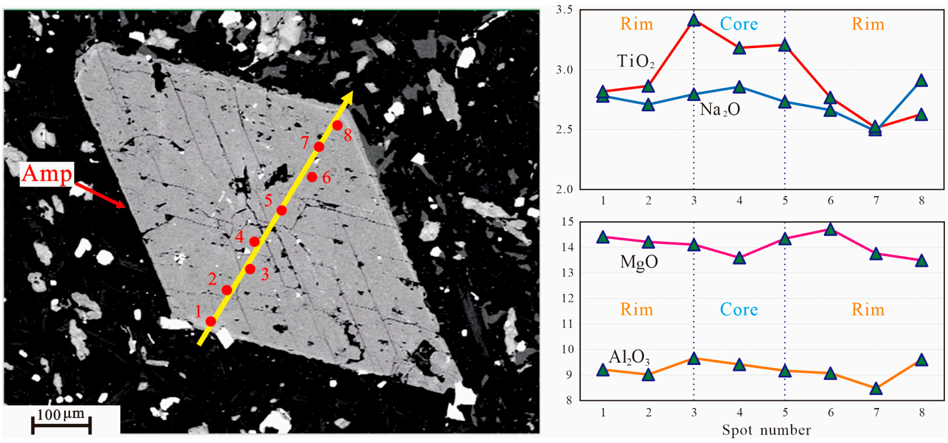

(a) (b)

Figure 7. Backscattered electron image characteristics (**a**) and electron probe analysis results (**b**) of the amphibole from the MMEs.

The temperature of amphibole crystallization in the MMEs was calculated using the amphibole thermometer formula proposed by Putirka (2016) [24]: T/°C = 1781 − 132.74Si + 116.6Ti − 69.41Fe^T + 101.62Na (±30 °C). The calculated temperature range for amphibole crystallization was 876–985 °C (Supplementary Table S4). According to the manometer formula based on the overall composition of amphibole proposed by Ridolfi and Renzulli (2012) [25], lnP(MPa) = 38.723 − 2.6957Si − 2.3565Ti − 1.3006Al − 2.7780Fe − 2.4838Mg − 0.6614Ca − 0.2705Na + 0.1117K. The pressure during amphibole crystallization was calculated to be 126–223 MPa. Using P = ρgH, the formation depth of the amphibole in the MMEs was calculated to be 4.76–8.43 km (Supplementary Table S4).

4.3.3. Biotite

EMPA analysis was performed in representative biotites of both the host granite and MMEs. The representative compositions and biotite formulae are provided in Supplementary Table S5. Biotites in the MMEs show slightly more TiO_2 and MgO contents than the host rocks. The FeO and Al_2O_3 contents are relatively high in the host rocks. The Mg/(Mg + Fe^{2+}) ratios of biotite in the host rock and MMEs are 0.33–0.70 and 0.61–0.73, respectively. The biotite in the host granite exhibits characteristics of being rich in iron and magnesium, while the biotite in the MMEs exhibits a characteristic of being rich in magnesium. In the Mg−(Al^{VI} + Fe^{3+} + Ti)−(Fe^{2+} + Mn) classification diagram of biotite, the biotite in the host rock falls into the Mg-biotite and Fe-biotite areas, while the biotite composition in the MMEs falls into the Mg-biotite area (Figure 5c) [22]. In the 10TiO_2−FeO + MnO)−MgO diagram, the biotites from the host rock and the MMEs all fall within the area of primary biotite (Figure 5d) [23], suggesting that the biotite was not altered by late-stage hydrothermal fluids but was a product of magmatic activity.

Biotite can be used as an effective indicator to reflect the temperature and pressure during magma crystallization. The Ti-in-biotite thermometer for biotite proposed by Henry et al. (2005) [26] was used to estimate the crystallization temperature of magma: $T/°C = \{[\ln(Ti) - a - c(X_{Mg})^3]/b\}^{0.333}$, where a = −2.3594, b = 4.6482 × 10^{-9}, and c = −1.7283, X_{Mg} = Mg/(Mg + Fe). The X_{Mg} and Ti values of biotite in the host granite are 0.33–0.63 and 0.37–0.57, respectively, while those in the MMEs are 0.55–0.64 and 0.33–0.58, respectively. The calculated crystallization temperatures of biotite in the host rock and MMEs are 687–752 °C and 705–764 °C, respectively (Supplementary Table S5). It can be seen that the crystallization temperature of biotite in the MMEs is higher than that in the host granite, indicating that the MMEs have more mafic magma components involved in their formation compared to the host rock.

5. Discussion

5.1. Petrogenesis of Langqi Pluton

The widely developed MMEs in the granite are often regarded as direct evidence of magma mixing [6,8]. Overall, most of the MMEs in the Langqi granite are lens-shaped or ellipsoidal (Figure 2a–f), indicating that they were products of mafic magma injected into the felsic magma and underwent plastic deformation. The contacts between the MMEs and the host granite are mostly sharp, implying that the temperature of the mafic magma was significantly higher than that of the felsic magma, and that when both magmas mixed, quenching and crystallization were likely to occur [27]. The MMEs exhibit a smaller mineral particle diameter in comparison to the host rock, signifying that the mafic magma experienced rapid cooling upon intrusion into the lower-temperature felsic magma, resulting in a shorter crystallization time and smaller grain size in the MMEs [28,29]. In the field, plagioclase phenocrysts in the MMEs exhibit comparable shapes and sizes to those present in the host rock (Figure 2a,c), indicating that these plagioclase phenocrysts in the MMEs were not formed in situ but were captured by the mafic magma from the felsic magma during the magmatic mixing process. Furthermore, a phenomenon was observed in the field where larger MMEs enveloped smaller MMEs (Figure 2b,d). This could be related to the injection of mafic magma into hybrid magma layers, which were subsequently injected into the felsic magma [30]. In the MMEs, needle-shaped apatite is still visible (Figure 3i), which also indicates a rapid condensation process of high-temperature mafic magma encountering lower-temperature felsic magma [31,32]. In addition, there are multiple mineral disequilibrium textures and mineral associations in the MMEs, such as the poikilitic inclusions of amphibole within the plagioclase with a chaotic texture (Figure 3d) or an oscillatory zoning pattern (Figure 3f,h). These phenomena of mineral disequilibrium textures and mineral associations cannot be explained by the normal order of crystallization, indicating that the MMEs were formed by the mixing of mantle-derived mafic magma and crust-derived felsic magma. The evidence presented at both the macro- and micro-scales indicates that the Langqi pluton has a characteristic of magma mixing origin.

The zircon U-Pb dating of the Langqi MMEs indicates a formation age of 98.9 ± 2.2 Ma, which is consistent with the age of the granites (100.1 ± 1.1 Ma) reported by Huang et al. (2020) [10] within the error range (Figure 4). Both were emplaced in the late Early Cretaceous, ruling out the possibility that the MMEs are either refractory residues or xenoliths from the wall rocks, as the formation age of both should be significantly earlier than that of the host granites. These geochronological results further suggest that the Langqi granites and MMEs are products of simultaneous crystallization and magma mixing [28,29].

Although Hf isotopes are difficult to diffuse and homogenize in magma, they can record this homogenization process [33]. The εHf(t) values of zircons in the Langqi granite range from −2.1 to 0.0, while those in the MMEs range from −1.7 to +1.1 (Supplementary Table S2). Both have similar εHf(t) values, indicating the significant influence of magma mixing on both the granites and the MMEs. Based on the study of the major and trace elements of the Langqi pluton by Huang et al. (2020) [10], the $CaO/Al_2O_3-K_2O/MgO$, $Al_2O_3/CaO-Na_2O/CaO$, and Cr-Ni diagrams show good covariation between the compositions of the granite and the MMEs, and the host rocks and the MMEs have similar rare-earth distribution curves and trace element characteristics, indicating that the Langqi pluton was formed by the mixing of mafic magmas and felsic magmas.

5.2. Mineralogical Records of the Magma Mixing Process

5.2.1. Inversion of Magmatic Processes by Chemical Zoning of Plagioclase

The chemical zoning of plagioclase can fully record the changes in magma composition during its crystallization, which is an important way to understand the mechanism of magma's evolution [34]. The plagioclase phenocrysts in MMEs exhibit a clear oscillatory zoning pattern (Figure 3f,h), with the core having a relatively more calcic composition and the An values showing an oscillatory change phenomenon of "alternately decreasing and increasing" from the core to the rim (Figure 6). This indicates that the continuous variation in An values from the core to the rim of plagioclase may be the result of multiple pulsating mixing events between two different components of magma [35]. As magma mixing becomes more complete and the temperature decreases, the An values at the rim of the plagioclase steadily decrease, showing the phenomenon of a normal zoning pattern. The normal zoning pattern of plagioclase is considered to be the crystallization product of a more homogeneous magma composition, reflecting the shift in magma composition from mafic to felsic. This is because the surface of the earlier-crystallized plagioclase is enveloped by the later-crystallized plagioclase with higher Ab contents, resulting in higher Ab contents at the rim compared to the core [36]. The microlites in the matrix of the MMEs show slightly lower An values compared to those at the rim of the plagioclase phenocrysts, indicating the crystallization of microlites during the cooling [37]. The mixing of mafic magmas and felsic magma also resulted in partial overlap of the An values of plagioclase in the granite and MMEs (Figure 5a). In addition, sieve textures are commonly developed in the plagioclase phenocrysts from the MMEs, in which the poikilitic inclusions of amphibole are encased (Figure 3d). This can be attributed to the heat and material exchange during the injection of high-temperature mafic magma into cooler felsic magma, which caused volatiles in the magma to escape and led to the destruction of the early-formed plagioclase texture, followed by partial melting corrosion. The poikilitic inclusions of amphibole then filled the melting embayments and holes of the plagioclase.

5.2.2. Mafic Minerals' Constraints on the Magma Mixing Processes

Amphibole is one of the common rock-forming minerals in magmatic rocks. Previous research has shown that the Ti content in the amphibole is not only related to the temperature during crystallization but also controlled by the chemical composition of the magma [38]. The whole-rock TiO_2 contents of the host rocks ranged from 0.26% to 0.29%, while those of the MMEs ranged from 0.71% to 1.44% [10], which is much higher than that of the host rock. Therefore, the Ti content in the Langqi pluton is mainly controlled by the chemical composition of the magma of the MMEs (Figure 7), and the TiO_2 contents at the core of amphibole are significantly higher than at the rim. Additionally, the distribution of the TiO_2 contents from the core to the rim is uneven, indicating that during the formation of the amphibole phenocrysts in the MMEs, a reaction with a low-Ti-containing melt led to decreased Ti contents in the rim of the amphibole phenocrysts relative to the core. The poikilitic inclusions of plagioclase within the amphibole with a long columnar shape (Figure 3e,g) indicate that the low-Ti melt composition may be related to felsic magma in this study. Taking into account the aforementioned characteristics, it appears that during the magma mixing process between mantle-derived mafic magmas and crust-derived felsic magmas, due to the presence of concentration differences, the TiO_2 contents migrated from the mafic magma with higher TiO_2 concentrations to the felsic magma with lower TiO_2 concentrations [39].

The amphiboles in the MMEs belong to the calciferous amphibole. Previous studies have shown that the Si, Ti, and Al contents in calciferous amphibole exhibit regular variations with different magma source regions, where the Si/(Si + Ti + Al) ratio for crust-derived amphibole is $\geq$0.775, while for mantle-derived amphibole it is $\leq$0.765 [40]. The Si/(Si + Ti + Al) ratios of the amphibole in the MMEs in this study ranged from 0.728 to 0.795, showing some characteristics of the mantle–crust mixing type. In the TiO_2–Al_2O_3 diagram for amphibole, most of the amphiboles in the MMEs are situated in the mantle source area close to the crust–mantle mixing boundary, with a few located within the crust–mantle mixing area [40] (Figure 8a). This trend is consistent with the Si/(Si + Ti + Al) ratios of the amphibole. These results indicate, to some extent, that the amphibole in the MMEs is the product of residual magma crystallization subsequent to the injection of mantle-derived mafic magma into felsic magma during magma mixing.

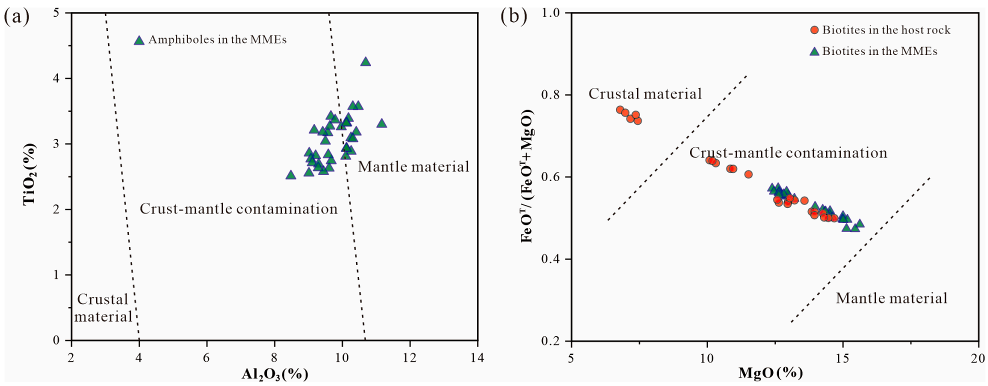

Figure 8. Origin diagram of amphiboles from the MMEs ((**a**), after Jiang and An, 1984) [40] and origin diagram of biotites from the host granite and MMEs ((**b**), after Guo et al., 2017) [41].

The chemical composition of biotite is related to the tectonic environment, and its characteristic composition can reflect the genetic type and formation environment of the host rock. Previous research results have shown that the MF (=Mg/(Mg + Fe + Mn)) of biotite in I-type granite is greater than 0.38, while the MF of biotite in S-type granite is less than 0.38 [42]. The MF values of biotite in the host granite and MMEs are 0.32–0.60 and 0.54–0.63, respectively, indicating that they belong to the I-type granite series. Based on the analysis of the major elemental data of biotite in different tectonic environments of igneous rocks, biotites from the host granite and the MMEs fall within the calc-alkaline region of the orogenic belt, related to subduction in the discriminant diagram of the tectonic environment for biotites proposed by Abdel-Rahman (1994) [43] (Figure 9). As calc-alkaline rocks in orogenic belts are mostly I-type granites, this further indicates that the granites in the study area have mineral chemical characteristics of the I-type granite series, which is consistent with the results obtained by Huang et al. (2020) [10] using whole-rock geochemical analysis. Previous studies have also shown that I-type granitic rocks are mainly derived from the remelting of intermediate–basic igneous rocks from the middle and lower crust that have not undergone weathering, and their formation process may involve contamination with mantle-derived components or other crustal materials [44,45].

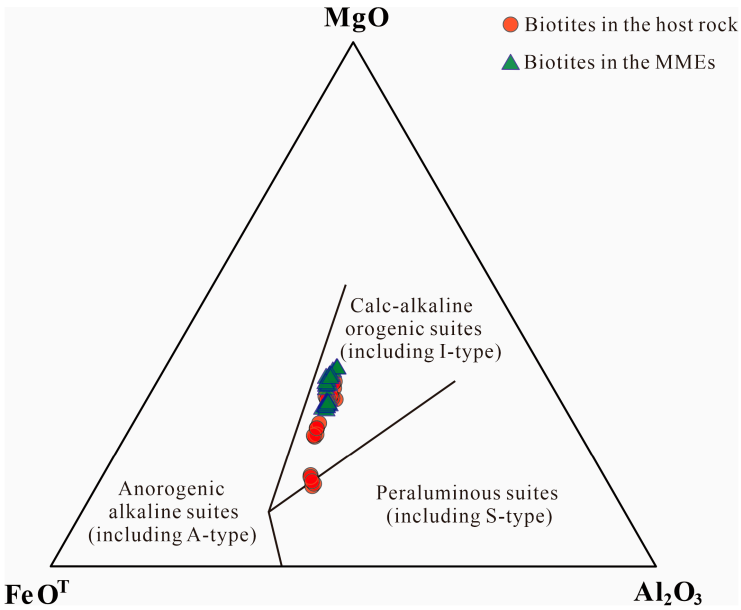

Figure 9. Discriminant diagram of the tectonic environment for biotites from the host granite and MMEs (after Abdel-Rahman, 1994) [43].

The MgO contents of the biotites in the host rock and MMEs ranged from 6.79% to 14.68% and from 12.39% to 15.62%, respectively, showing certain mantle-derived magma characteristics. In the $MgO-FeO^T/(MgO + FeO^T)$ diagram, a minority of biotites in the host rock fall in the crustal source area, while the majority fall in the crust–mantle mixing area. All biotites in the MMEs fall in the crust–mantle mixing area [41] (Figure 8b), indicating to some extent that the biotites in both the host rock and the MMEs are products formed by the mixing of mafic magma and felsic magma.

The crystallization temperature, pressure, and formation depth of amphibole crystals in the MMEs range from 876 to 985 °C, from 126 to 223 MPa, and from 4.76 to 8.43 km, respectively (Supplementary Table S4), indicating that they were formed at greater depths and at an earlier time. The crystallization temperatures of biotites in the MMEs (705–764 °C) are higher than those of biotites in the host rock (687–752 °C; Supplementary Table S5), indicating that the biotites in the host rock formed at a later time. Based on this, the authors believe that the felsic magma is penetrated by foreign mafic magma in the process of crystallization, and that the mixed magma crystallized amphibole around the previously formed plagioclase in the felsic magma, resulting in the phenomenon of the poikilitic inclusions of plagioclase within the amphibole from the MMEs (Figure 3e,g). As the mantle–crust mixed magma continued to intrude and cool, the biotites began to crystallize in the MMEs. When the mixed magma continued to rise for a period of time, the biotites in the host rock crystallized.

5.3. Mechanism of Magma Mixing

The extensive Mesozoic magmatic activity observed in the southeast coastal region of China is considered to be intimately linked to the subduction of the Paleo-Pacific Plate towards the Eurasian continent [15]. Early Jurassic granites and contemporaneous mantle-derived rocks appeared in large volumes along the eastern coast, indicating that the subduction of the Paleo-Pacific Plate had already begun in the Early Jurassic [46,47]. During the Middle Jurassic to Early Cretaceous, the Paleo-Pacific Plate gradually changed into high-angle subduction due to gravitational drag [48]. The steeper subduction angle caused a strong sinistral strike-slip activity in the Changle-Nan'ao Fault Zone, resulting in the intrusion of the mantle-derived magma with large-scale contamination of crustal material. Migmatization occurred near the Changle-Nan'ao Fault Zone [49]. The widespread occurrence of Late Cretaceous A-type granites in the coastal areas of Fujian Province [5,17] and the contemporaneous mafic dyke swarms [14] indicate that the compressive environment in the area changed to an extensional environment caused by the rollback of the Paleo-Pacific Plate in the last period of the Early Cretaceous. The occurrence of granites and metamorphic rocks in the Changle-Nan'rao Fault Zone indicates that large-scale magmatic activity (116~90 Ma) and metamorphism (~108 Ma) are related to the post-collisional extensional environment [50,51]. The gradual increase in extension and thinning of the lithosphere has led to an increasing contribution of mafic magma, which can not only act as a heat source but also mixes with crustal material to varying degrees.

The Langqi pluton is classified as I-type granite and exhibits characteristics of high silicon, high potassium, alkali richness, and low magnesium. All samples of the Langqi granite and MMEs had zircon εHf(t) values ranging from −2.1 to 0.0 and from −1.7 to +1.1, respectively, displaying enriched features, and all were located above the ancient basement of the Cathaysia Block (Figure 10). Both the host granite and the MMEs have two-stage model ages (T_{DM2}) ranging from 1162 to 1289 Ma and from 1089 to 1269 Ma, respectively, which are significantly younger than the age of the ancient basement of the Cathaysia Block (1.85~1.87 Ga, 2.10~2.40 Ga) [52]. This suggests the occurrence of significant magma mixing during the formation process of the Langqi pluton. The geochemical features of the Langqi granites are similar to those of contemporaneous granite rocks in the same region, such as the Danyang and Puqian plutons. They exhibit enriched Hf isotopic compositions (with εHf(t) around −5 and T_{DM2} around 1000 Ma) and low $\delta^{18}O$ values (with $\delta^{18}O$ values around 4.5‰). Their parental magma formed by the mixing of felsic magmas derived from the partial melting of mafic rocks with low $\delta^{18}O$ characteristics and mafic magmas derived from the mantle (or juvenile crust), followed by fractional crystallization and involvement of the ancient continental crust [53].

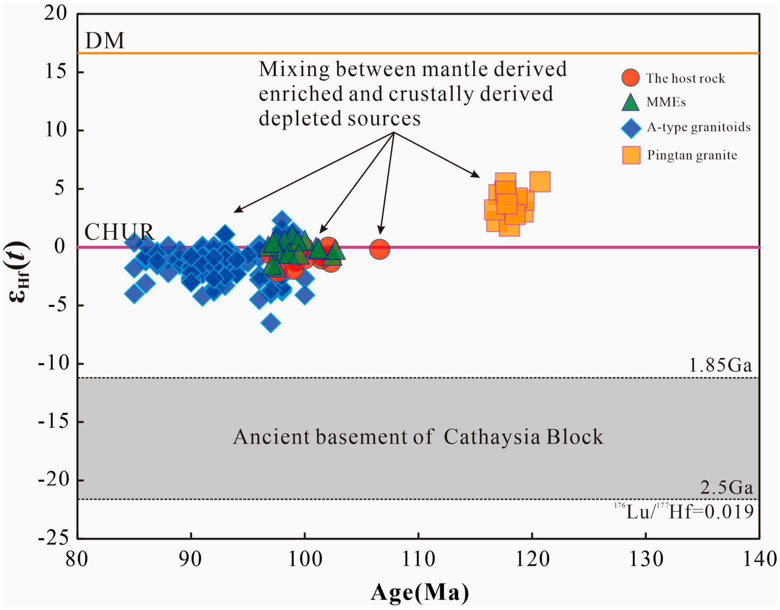

Figure 10. U−Pb ages versus εHf(t) diagram of zircons from the host granite and MMEs: The Hf isotope evolution of the Cathaysia crustal basement (after He and Xu, 2012) [16], A-type granitoids, and Pingtan granite data are cited from Zhao et al. (2015) [54], Chen et al. (2019) [17] and Zhang et al. (2020) [55].

The Late Cretaceous A-type granitoids located on the southeastern coast of Fujian Province (εHf(t) ranges from −6.5 to +4.2) were studied by previous researchers, who concluded that the formation of these A-type granitoids was related to the gradually intensifying regional extension caused by the rollback of the subducted Paleo-Pacific Plate [17,54]. In the U-Pb ages vs. εHf(t) diagram of zircons from the host rock and MMEs, the εHf(t) values of the Langqi pluton are very similar to those of the A-type granitoids (Figure 10), suggesting that the Langqi pluton was formed in a back-arc extensional tectonic setting due to the mixing of the mantle-derived magma and subsequently induced crustal felsic magma by underplating, which is consistent with the conclusion reached by Huang et al. (2020) [10]. Zhang et al. (2020) [55] proposed that the melting source region of the Pingtan Island granite (117.4 ± 1.0 Ma; εHf(t) ranges from +1.8 to +5.6) is mainly from new crustal material, with a relatively small contribution from the ancient basement of the Cathaysia Block. The U-Pb ages vs. εHf(t) diagram of zircons from the Langqi pluton reveals that all of the εHf(t) values of the former are located below those of the Pingtan Island granites (Figure 10), indicating that during the formation process of the Langqi pluton, the contribution of the ancient basement of the Cathaysia Block to it was relatively higher than that to the Pingtan Island granites. Moreover, the Langqi granites are more enriched than the MMEs, suggesting that the ancient basement of the Cathaysia Block played a relatively more significant role in the formation of the Langqi granites than in that of the MMEs.

The explanation of the origin of mafic dikes or veins using the crystal mushy magma system has been increasingly recognized by scholars [8,27,56,57]. The crystal mushy magma system is characterized by a felsic magma chamber with an upper melt-rich layer containing few crystals and a lower crystal-rich layer containing a large number of early crystallized mineral crystals (the crystal content is more than 40%). When mafic magma intrudes into the melt-rich layer of the crystal mushy magma system, it is difficult for it to undergo mixing interaction or only mingling interaction due to its lower temperature, higher density, and non-Newtonian rheological behavior, and mafic dikes or veins are often formed. However, if the mafic magma intrudes upward into the well-flowing melt-rich layer, chemical mixing is more likely to occur. Based on this, it is speculated that the Langqi doleritic veins (Figure 2g–i) were formed by the intrusion of the mantle-derived magma into the crystal-rich layer of the crystal mushy magma reservoir.

In summary, this article posits that in the late Early Cretaceous, the rollback of the Paleo-Pacific Plate resulted in the intrusion of mantle-derived magmas into the ancient basement of the Cathaysia Block. This process caused the mobilization of the overlying crustal felsic crystal mushy magma chamber. Some of the mafic magmas were injected into the crystal-rich layer of the felsic magma chamber. The Langqi doleritic veins formed due to the differing non-Newtonian rheological behavior and rapid cooling and crystallization. As the mafic magma continued to intrude and entered the transitional zone between the crystal-rich and melt-rich layers of the felsic magma chamber, the mixing interaction between the mafic magma and felsic magma led to the almost simultaneous formation of the Langqi granites and MMEs. During this process, mantle-derived mafic magma contributed more to the formation of the MMEs than to that of the granites. The mixing interaction of crust–mantle magma in a crystal mushy state is an important way to control the formation and evolution of the Langqi pluton in different proportions and manners.

6. Conclusions

1. The formation age of the MMEs from Langqi pluton is 98.9 $\pm$ 2.2 Ma, which is consistent with the age of the granite (100.1 $\pm$ 1.1 Ma) within the error range. This suggests that the MMEs are not refractory residues or xenoliths from the wall rocks but are products of magma mixing. The zircon εHf(t) values of the granite and MMEs range from -2.1 to 0.0 and from -1.7 to +1.1, respectively, with corresponding two-stage model ages (T_{DM2}) of 1162–1289 Ma and 1089–1269 Ma, respectively, indicating that their magma source is mainly derived from the ancient basement of the Cathaysia Block, with some contribution from mantle materials.
2. The oscillatory variation in An values from the core to the rim of the plagioclase phenocryst with an oscillatory zoning pattern in the MMEs, showing a pattern of alternating decrease and increase, may be the result of multiple pulsating mixing events between two different magma components. The amphiboles in the MMEs display certain characteristics of mantle–crust mixing. The TiO_2 contents from the core to the rim exhibit an uneven pattern, with higher contents in the core and lower contents in the rim, indicating a migration of TiO_2 from the mafic magma with high concentration to the felsic magma with low concentration. The biotites in the host rock and MMEs are both primary biotites with features of mantle–crust mixing.
3. The Langqi pluton was formed in the context of plate subduction, and some mafic magmas intruded into the crystal-rich layer of the felsic crystal mushy magma chamber to form doleritic veins. When the mafic magma entered the transitional zone between the crystal-rich and melt-rich layers of the felsic magma chamber, it underwent varying degrees of mixing interaction with the felsic magma, resulting in the formation of the granites and MMEs.

Supplementary Materials: The following supporting information can be downloaded at: https://www.mdpi.com/article/10.3390/min13121538/s1, Table S1: LA-ICP-MS zircon U-Pb analytical results of the MMEs; Table S2: Zircon Hf isotope compositions of the host rock and MMEs; Table S3: Representative EPMA of the chemical composition (wt.%) and calculated formula of plagioclase in the host rock and MMEs; Table S4: Representative EPMA of the chemical composition (wt.%) and calculated formula of amphibole in the MMEs; Table S5: Representative EPMA of the chemical composition (wt.%) and calculated formula of biotite in the host rock and MMEs.

Author Contributions: Conceptualization, Z.C. and L.W.; methodology, Z.C.; validation, L.W.; formal analysis, L.W.; investigation, X.Y.; resources, L.W.; data curation, Z.C.; writing—original draft

preparation, Z.C.; writing—review and editing, L.W.; supervision, X.Y.; funding acquisition, L.W. All authors have read and agreed to the published version of the manuscript.

Funding: This research was financially supported by the National Natural Science Foundation of China (Grant Nos: 42230807, 41903007, 41873012).

Data Availability Statement: Data are contained within the article and supplementary material.

Acknowledgments: The authors would like to thank Musen Lin for help with fieldwork and Suyu Chen for help with EPMA and many discussions. Finally, we are grateful to the editor and the three reviewers.

Conflicts of Interest: The authors declare no conflict of interest.

References

1. Li, Z.; Qiu, J.S.; Yang, X.M. A review of the geochronology and geochemistry of Late Yanshanian (Cretaceous) plutons along the Fujian coastal area of southeastern China: Implications for magma evolution related to slab break-off and rollback in the Cretaceous. *Earth-Sci. Rev.* **2014**, *128*, 232–248. [CrossRef]
2. Li, S.Z.; Suo, Y.H.; Li, X.Y.; Wang, Y.M.; Cao, X.Z.; Wang, P.C.; Guo, L.L.; Yu, S.Y.; Lan, H.Y.; Li, S.J.; et al. Mesozoic plate subduction in West Pacific and tectono-magmatic response in the East Asian ocean-continent connection zone. *Chin. Sci. Bull.* **2018**, *63*, 1550–1593. (In Chinese with English abstract) [CrossRef]
3. Liu, J.X.; Wang, S.; Wang, X.L.; Du, D.H.; Xing, G.F.; Fu, J.M.; Chen, X.; Sun, Z.M. Refining the Spatio-Temporal Distributions of Mesozoic Granitoids and Volcanic Rocks in SE China. *J. Asian Earth Sci.* **2020**, *201*, 104503. [CrossRef]
4. Guo, F.; Zhao, L.; Zhang, X.B.; Wu, Y.M.; Zhang, B.; Zhang, F. Geodynamics of Late Mesozoic Magmatism in the Eastern South China Block: An Overview. *Geotecton. Metallog.* **2022**, *46*, 416–434. (In Chinese with English abstract)
5. Zhao, J.L.; Qiu, J.S.; Liu, L.; Wang, R.Q. The Late Cretaceous I- and A-type granite association of southeast China: Implications for the origin and evolution of post-collisional extensional magmatism. *Lithos* **2016**, *240*, 16–33. [CrossRef]
6. Vernon, R.H. Microgranitoid enclaves in granites: Globules of hybrid magma quenched in a plutonic environment. *Nature* **1984**, *309*, 438–439. [CrossRef]
7. Dorais, M.J.; Whitney, J.A.; Roden, M.F. Origin of mafic enclaves in the Dinkey Creek pluton, central Sierra Nevada batholith, California. *J. Petrol.* **1990**, *31*, 853–881. [CrossRef]
8. Barbarin, B. Mafic magmatic enclaves and mafic rocks associated with some granitoids of the central Sierra Nevada batholith, California: Nature, origin, and relations with the hosts. *Lithos* **2005**, *80*, 155–177. [CrossRef]
9. Mo, X.X. Magma and Magmatic/Igneous Rocks: A Lithoprobe into the Deep Earth and Records of the Earth's Evolution. *Chin. J. Nat.* **2011**, *33*, 255–259. (In Chinese with English abstract)
10. Huang, L.L.; Wang, L.Y.; Fan, H.R.; Lin, M.S.; Zhang, W.H. Late Early-Cretaceous Magma Mixing in the Langqi Island, Fujian Province, China: Evidences from Petrology, Geochemistry and Zircon Geochronology. *J. Earth Sci.* **2020**, *31*, 468–480. [CrossRef]
11. Guo, Y.Y.; He, W.Y.; Li, Z.C.; Ji, X.Z.; Han, Y.; Fang, W.K.; Yin, C. Petrogenesis of Ge'erkuohe porphyry granitoid, western Qinling: Constraints from mineral chemical characteristics of biotites. *Acta Petrol. Sin.* **2015**, *31*, 3380–3390. (In Chinese with English abstract)
12. He, W.Y.; Mo, X.X.; He, Z.H.; White, N.C.; Chen, J.B.; Yang, K.H.; Wang, R.; Yu, X.H.; Dong, G.C.; Huang, X.F. The geology and mineralogy of the Beiya Skarn gold deposit in Yunnan, Southwest China. *Econ. Geol.* **2015**, *110*, 1625–1641. [CrossRef]
13. Yang, L.Q.; Deng, J.; Qiu, K.F.; Ji, X.Z.; Santosh, M.; Song, K.R.; Song, Y.H.; Geng, J.Z.; Zhang, C.; Hua, B. Magma mixing and crust-mantle interaction in the Triassic monzogranites of Bikou Terrane, central China: Constraints from petrology, geochemistry, and zircon U-Pb-Hf isotopic systematics. *J. Asian Earth Sci.* **2015**, *98*, 320–341. [CrossRef]
14. Ding, C.; Zhao, Z.D.; Yang, J.B.; Zhou, H.F.; Sheng, D.; Hou, Q.Y.; Hu, Z.C. Geochronology, geochemistry of the Cretaceous granitoids and mafic to intermediate dykes in Shishi area, coastal Fujian Province. *Acta Petrol. Sin.* **2015**, *31*, 1433–1447. (In Chinese with English abstract)
15. Zhou, X.M.; Sun, T.; Shen, W.Z.; Shu, L.S.; Niu, Y.L. Petrogenesis of Mesozoic granitoids and volcanic rocks in South China: A response to tectonic evolution. *Episodes* **2006**, *29*, 26–33. [CrossRef]
16. He, Z.Y.; Xu, X.S. Petrogenesis of the Late Yanshanian mantle-derived intrusions in southeastern China: Response to the geodynamics of paleo-Pacific plate subduction. *Chem. Geol.* **2012**, *328*, 208–221. [CrossRef]
17. Chen, J.Y.; Yang, J.H.; Zhang, J.H. Origin of Cretaceous aluminous and peralkaline A-type granitoids in northeastern Fujian, coastal region of southeastern China. *Lithos* **2019**, *340*, 223–238. [CrossRef]
18. Wang, L.Y.; Peng, X.D.; Huang, L.L.; Lin, M.S.; Zhang, W.H. Petrogenesis and geological implications of the Changanshan diorite and rhyolite in Minhou area, Fuzhou. *Acta Petrol. Sin.* **2020**, *36*, 1833–1849. (In Chinese with English abstract)
19. Liu, Y.S.; Hu, Z.C.; Gao, S.; Günther, D.; Xu, J.; Gao, C.G.; Chen, H.H. In situ analysis of major and trace elements of anhydrous minerals by LA-ICP-MS without applying an internal standard. *Chem. Geol.* **2008**, *257*, 34–43. [CrossRef]
20. Wu, F.Y.; Yang, Y.H.; Xie, L.W.; Yang, J.H.; Xu, P. Hf isotopic compositions of the standard zircons and baddeleyites used in U-Pb geochronology. *Chem. Geol.* **2006**, *234*, 105–126. [CrossRef]

21. Leake, B.E.; Woolley, A.R.; Arps, C.E.S.; Birch, W.D.; Gilbert, M.C.; Grice, J.D.; Hawthorne, F.C.; Kato, A.; Kisch, H.J.; Krivovichev, V.G.; et al. Nomenclature of Amphiboles: Report of the Subcommittee on Amphiboles of the International Mineralogical Association Commission on New Minerals and Mineral Names. *Can. Mineral.* **1997**, *35*, 219–246.
22. Forster, M.D. Interpretation of the composition of trioctahedral micas. *Geol. Surv. Prof. Pap.* **1960**, *354*, 11–49.
23. Nachit, H.; Ibhi, A.; Abia, E.H.; Ben Ohoud, M. Discrimination between primary magmatic biotites, reequilibrated biotites and neoformed biotites. *Comptes Rendus Geosci.* **2005**, *337*, 1415–1420. [CrossRef]
24. Putirka, K. Amphibole thermometers and barometers for igneous systems and some implications for eruption mechanisms of felsic magmas at arc volcanoes. *Am. Mineral.* **2016**, *101*, 841–858. [CrossRef]
25. Ridolfi, F.; Renzulli, A. Calcic amphiboles in calc-alkaline and alkaline magmas: Thermobarometric and chemometric empirical equations valid up to 1130 °C and 2.2 Gpa. *Contrib. Mineral. Petrol.* **2012**, *163*, 877–895. [CrossRef]
26. Henry, D.J.; Guidotti, C.V.; Thomson, J.A. The Ti-saturation surface for low-to-medium pressure metapelitic biotites: Implications for geothermometry and Ti-substitution mechanisms. *Am. Mineral.* **2005**, *90*, 316–328. [CrossRef]
27. Chen, B.; Xiong, F.H.; Ma, C.Q.; Chen, Y.; Huang, H. Coupling relation between magma mixing and igneous petrological diversity: An example of Bairiqili felsic pluton in East Kunlun Orogen. *Earth Sci.* **2020**, *46*, 2057–2072. (In Chinese with English abstract)
28. Wiebe, R.A.; Smith, D.; Sturm, M. Enclaves in the Cadillac mountain granite (coastal Maine): Samples of hybrid magma from the base of the chamber. *J. Petrol.* **1997**, *38*, 393–423. [CrossRef]
29. Kumar, S.; Rino, V. Mineralogy and Geochemistry of Microgranular Enclaves in Palaeoproterozoic Malanjkhand Granitoids, Central India: Evidence of Magma Mixing, Mingling, and Chemical Equilibration. *Contrib. Mineral. Petrol.* **2006**, *152*, 591–609. [CrossRef]
30. Kumar, S.; Pieru, T. Petrography and major elements geochemistry of microgranular enclaves and Neoproterozoic granitoids of South Khasi, Meghalaya: Evidence of magma mixing and alkali diffusion. *J. Geol. Soc. India* **2010**, *76*, 345–360. [CrossRef]
31. Niu, M.L.; Wen, F.L.; Yan, Z.; Wu, Q.; Li, X.C.; Sun, Y.; Li, C. Early Paleozoic magma mixing in the Lajishan tectonic belt of South Qilian: An example from the Machang pluton. *Acta Petrol. Sin.* **2021**, *37*, 2364–2384. (In Chinese with English abstract)
32. Song, B.; Wang, B.W.; Xu, W.; Niu, Y.Z.; Zhang, Q.; Gou, H.G.; Yan, Q.R. Net Growth of the Continental Crust during the Process of Accretionary Orogeny: Constraints from Igneous Rocks, Southern Margin of the Middle Section of the Central Asian Orogenic Belt. *Acta Petrol. Sin.* **2021**, *37*, 1044–1060. (In Chinese with English abstract)
33. Wang, X.L.; Wang, D.; Du, D.H.; Li, J.Y. Diversity of Granitic Rocks Constrained by Disequilibrium Melting and Subsequent Incremental Emplacement and Differentiation. *Lithos* **2021**, *402*, 106255. [CrossRef]
34. Lu, T.Y.; He, Z.Y.; Zhang, Z.M.; Shui, X.F.; Yan, L.L. Magma mixing of the Nyemo post-collisional granite from the Gangdese magmatic belt, Tibet: Evidence of microstructures. *Acta Petrol. Sin.* **2016**, *32*, 3613–3623. (In Chinese with English abstract)
35. Zhang, R.G.; He, W.Y.; Gao, X.; Li, M.M. Magma mixing of the Daocheng batholith of western Sichuan: Mineralogical evidences. *Earth Sci. Front.* **2018**, *25*, 226–239. (In Chinese with English abstract)
36. Zeng, R.Y.; Lai, J.Q.; Zhang, L.J.; Ju, P.J. Petrogenesis of Mafic Microgranular Enclaves: Evidence from Petrography, Whole-Rock and Mineral Chemistry of Ziyunshan Pluton, Central Hunan. *Earth Sci.* **2016**, *41*, 1461–1478. (In Chinese with English abstract)
37. Hattori, K.; Sato, H. Magma evolution recorded in plagioclase zoning in 1991 Pinatubo eruption products. *Am. Mineral.* **1996**, *81*, 982–994. [CrossRef]
38. Molina, J.F.; Scarrow, J.H.; Montero, P.G.; Bea, F. High-Ti amphibole as a petrogenetic indicator of magma chemistry: Evidence for mildly alkalic-hybrid melts during evolution of Variscan basic-ultrabasic magmatism of Central Iberia. *Contrib. Mineral. Petrol.* **2009**, *158*, 69–98. [CrossRef]
39. Lv, Q.L.; Liu, J.F.; Zhao, S.; Guo, C.L.; Che, Y.W. Magma mixing mechanism of the Jiefangyingzi granodiorite in Inner Mongolia: Evidence from mineral chemistry of plagioclase and amphibole. *Acta Petrol. Mineral.* **2022**, *41*, 322–338. (In Chinese with English abstract)
40. Jiang, C.Y.; An, S.Y. On chemical characteristics of calcic amphiboles from igneous rocks and their petrogenedid significance. *J. Mineral. Petrol.* **1984**, *4*, 1–9. (In Chinese with English abstract)
41. Guo, N.X.; Wang, D.H.; Zhao, Z.; Chen, Y.C.; Chen, W.; Xie, X.W. Mineral characteristics of the Jiulongnao granite batholith in Southern Jiangxi Province and its indication of magma evolution and mineralization. *Earth Sci. Front.* **2017**, *24*, 76–92. (In Chinese with English abstract)
42. Xu, K.Q.; Sun, N.; Wang, D.Z.; Liu, C.S.; Chen, K.R. Two genetic series of granitic rocks in southeastern China. *Acta Petrol. Mineral. Anal.* **1982**, *1*, 1–12. (In Chinese with English abstract)
43. Abdel-Rahman, A.F.M. Nature of biotites from alkaline, calc-alkaline, and peraluminous magmas. *J. Petrol.* **1994**, *35*, 525–541. [CrossRef]
44. Wu, F.Y.; Li, X.H.; Yang, J.H.; Zheng, Y.H. Discussions on the petrogenesis of granites. *Acta Petrol. Sin.* **2007**, *23*, 1217–1238. (In Chinese with English abstract)
45. Gao, P.; Zheng, Y.F.; Zhao, Z.F. Experimental melts from crustal rocks: A lithochemical constraint on granite petrogenesis. *Lithos* **2016**, *266*, 133–157. [CrossRef]
46. He, Z.Y.; Xu, X.S.; Niu, Y.L. Petrogenesis and Tectonic Significance of a Mesozoic Granite-Syenite-Gabbro Association from Inland South China. *Lithos* **2010**, *119*, 621–641. [CrossRef]

47. Zhu, W.G.; Zhong, H.; Li, X.H.; He, D.F.; Song, X.Y.; Ren, T.; Chen, Z.Q.; Sun, H.S.; Liao, J.Q. The early Jurassic mafic–ultramafic intrusion and A-type granite from northeastern Guangdong, SE China: Age, origin, and tectonic significance. *Lithos* **2010**, *119*, 313–329. [CrossRef]
48. Zhou, Q.; Jiang, Y.H.; Liao, S.Y.; Zhao, P.; Jia, R.Y.; Liu, Z.; Wang, G.C.; Ni, C.Y. Pertrogenesis and tectonic implications of the late Jurassic basic rocks from the northern Shi-Hang zone, Southeast China. *Island Arc.* **2016**, *25*, 235–250. [CrossRef]
49. Du, J.Y. The Structural Features and Ages of Activities of Lianhuashan Fault and Changle-Nan'ao Fault. Ph.D. Thesis, Jilin University, Changchun, China, 2012. (In Chinese with English summary).
50. Li, Y.; Ma, C.Q.; Xing, G.F.; Zhou, H.W. The Early Cretaceous evolution of SE China: Insights from the Changle-Nan'ao Metamorphic Belt. *Lithos* **2015**, *230*, 94–104. [CrossRef]
51. Li, Y.; Ma, C.Q.; Xing, G.F.; Zhou, H.W.; Zhang, H.; Brouwer, F.M. Origin of a Cretaceous low-^{18}O granitoid complex in the active continental margin of SE China. *Lithos* **2015**, *216*, 136–147. [CrossRef]
52. Xu, X.S.; O'Reilly, S.Y.; Griffin, W.L.; Wang, X.L.; Pearson, N.J.; He, Z.Y. The crust of Cathaysia: Age, assembly and reworking of two terranes. *Precambrian Res.* **2007**, *158*, 51–78. [CrossRef]
53. Chen, J.Y.; Yang, J.H.; Zhang, J.H. Multiple sources of Cretaceous granitoids in northeastern Fujian, coastal area of southeastern China. *J. Asian Earth Sci.* **2019**, *182*, 103939. [CrossRef]
54. Zhao, J.L.; Qiu, J.S.; Liu, L.; Wang, R.Q. Geochronological, geochemical and Nd-Hf isotopic constraints on the petrogenesis of Late Cretaceous A-type granites from the southeastern coast of Fujian Province, South China. *J. Asian Earth Sci.* **2015**, *105*, 338–359. [CrossRef]
55. Zhang, B.; Guo, F.; Zhang, X.B. Petrogenesis of granitic rocks in the Pingtan Island, Fujian Province: Constraints from zircon U-Pb dating, O-Hf isotopes and biotite mineral chemistry. *Acta Petrol. Sin.* **2020**, *36*, 995–1014. (In Chinese with English abstract)
56. Ma, C.Q.; Zou, B.W.; Gao, K.; Wen, X. Crystal Mush Storage, Incremental Pluton Assembly and Granitic Petrogenesis. *Earth Sci.* **2020**, *45*, 4332–4351. (In Chinese with English abstract)
57. Xiong, F.H.; Ma, C.Q.; Chen, B.; Ducea, M.N.; Hou, M.C.; Ni, S.J. Intermediate-mafic Dikes in the East Kunlun Orogen, Northern Tibetan Plateau: A Window into Paleo-arc Magma Feeding System. *Lithos* **2019**, *340*, 152–165. [CrossRef]